Florence, Italy 12-16 July 2015
ICSV22
The 22nd International Congress on Sound and Vibration

A GREEN'S FUNCTION APPROACH TO THE STUDY OF HYSTERESIS IN A RIJKE TUBE

Alessandra Bigongiari and Maria Heckl

School of Computing and Mathematics, Keele University, ST55BG Keele, Newcastle-under-Lyme, Staffordshire,UK
e-mail: a.bigongiari@keele.ac.uk

The prediction of thermo-acoustic instabilities, causing large pressure oscillations, is fundamental in combustion systems such as domestic burners and industrial gas turbine engines as they cause thermal and mechanical stress to the equipment leading to premature wear or even critical damage. Hysteresis is a known phenomenon observed in the experimental study of thermo-acoustic oscillations in a duct, when a certain parameter (e.g. the heater position, heater power or pipe length) is varied. In order to understand the physical mechanism which causes hysteresis, we develop a model where the heat source is described by an FDF (flame describing function) and the acoustic field by a Green's function approach. The acoustic field has the form of a superposition of modes. We study the individual modes and their stability behavior. An individual mode i has two different (complex) frequencies, depending whether or not there is thermo-acoustic feedback: ω_i denotes the frequency for the no-feedback case, while Ω_i denotes the frequency of the heat-driven mode. The imaginary part of Ω_i is an indicator for the mode's stability. Stability maps are calculated for a range of heat-source positions and oscillation amplitudes. These are supplemented by time-history calculations, which reveal the evolution of the thermo-acoustic instabilities, in particular limit cycles and hysteresis. The results show that the model is able to predict hysteresis and to describe its dependence on system parameters.

1. Introduction

When a heat source, such as a flame or hot gauze, is placed into a duct, thermo-acoustic feedback can occur between the heat release and the acoustic field of the duct, which may result in the amplification of small amplitude perturbations. The study of the stability of the system to perturbations is fundamental to identify the operating conditions in which such instabilities can be avoided. Experimental [1,7], analytical [2] or numerical [8] investigations are commonly performed using simplified configurations/models for the burner, such as a Rijke tube, and the characteristics of acoustic oscillations are produced for different sets of pipe and heater parameters. In particular many experimental measurements [7] show evidence of hysteresis in pressure/velocity time series when a given parameter, such as the heater power or position, is gradually increased/decreased. In this paper we will present an analytical model, based on modal analysis and Green's function, to investigate the stability of the Rijke tube and the phenomenon of hysteresis. We will assume the acoustic field in the pipe to be one-dimensional and consider a compact heat source.

2. Model for the heat release

For a compact heat source, the heat release can be generally described by the following equation

$$q(x,t) = q(t)\delta(x - x_q), \tag{1}$$

where x_q is the source position and $q(x,t)$ is a local heat release rate (i.e. the heat release rate per unit mass) with units of power per unit mass.
For our analysis we will characterize the heat release rate using a Flame Describing Function (FDF), whose form is derived from experimental measurements [1] performed by the EM2C group at Ecole Centrale in Paris for a burner composed of a resonant cavity and a matrix flame.

Following [3], we can extrapolate a heat release law that fits the experimental data as follows. In the time domain the heat release law is written as

$$\frac{Q(t)}{\bar{Q}} = n_1 \frac{u(t-\tau)}{\bar{U}} - n_0 \frac{u(t)}{\bar{U}} \tag{2}$$

Where: Q and $\bar{Q}$ are the fluctuating and mean part of the heat release rate respectively, u and $\bar{U}$ are the acoustic velocity and mean flow, n_0 and n_1 are two constants that describe the heat release dependence on acoustic fluctuations and τ is a time lag. Rewriting equation (2) in the frequency domain we can derive the flame transfer function

$$\mathcal{T}(\omega) = n_1 e^{i\omega\tau} - n_0 , \tag{3}$$

and the gain

$$\left|\mathcal{T}(\omega)\right| = \sqrt{n_0^2 + n_1^2 - n_0 n_1 \cos\omega\tau} \tag{4}$$

In the experiment the acoustic velocity amplitude A, the frequency ω and the time lag τ were measured together with the maximum gain. Then, in order to compare with the measurement in [1], the constants n_0 and n_1 were chosen as follows

$$n_0 + n_1 = g_{\max} \qquad \text{and} \qquad n_0 - n_1 = 1 \tag{5}$$

in order to have a gain of 1 for $\omega = 0$ and the maximum of the gain g_{max} equal to the sum of the two constants. From the comparison it is possible to extrapolate an approximated analytical form both for g_{max} and τ, as a function of the normalized acoustic velocity amplitude $A/\bar{U}$:

$$g_{\max} = g_0 - g_1 \frac{A}{\bar{U}} \tag{6}$$

$$\tau = \tau_0 + \tau_2 \left(\frac{A}{\bar{U}}\right)^2 \tag{7}$$

We notice that we have a constant term, denoted by the subscript 0 and an amplitude dependent term: the maximum gain has a linear dependence on the perturbation amplitude, regulated by a factor g_1 and the time-lag has a quadratic dependence, multiplied by a factor τ_2. These expressions are valid approximations of the trend observed in [1] when the amplitude dependent term in equation (6) is not bigger than the constant g_0. Since we have introduced a dependence on the perturbation amplitude, the transfer function in equation (3) is now a FDF, $\mathcal{T}(\omega, A)$.

3. The Green's Function

The Green's function $G(x, x', t, t)$ is the velocity potential created by an impulsive point source located at *x'* and firing at *t'*. It is obtained as the solution of the governing equation

(8) $$\frac{1}{c^2}\frac{\partial^2 G}{\partial t^2}-\frac{\partial^2 G}{\partial x^2}=\delta(x-x')\delta(t-t'),$$

with the boundary conditions of the system under consideration, here a resonator with end conditions described by reflection coefficients R_0 at the inlet and R_L at the oulet. It consists of a superposition of modes, with modal amplitudes g_n and modal frequencies ω_n:

(9) $$G(x,x',t,t')=H(t-t')\Im\sum_{n=1}^{\infty}g_n(x,x')e^{-i\omega_n(t-t')}$$

The g_n and ω_n are calculated for different characteristics of the tube, modelling the end conditions and the eventual presence of a jump in the cross-sectional area [4], a blockage [5] or a temperature jump/gradient [6]. For the case of a sharp temperature jump, generated by the source at x_q, the tube is divided into two parts: a cold zone, upstream of the heat source, with speed of sound $c=c_1$ and a hot zone, downstream, with speed of sound $c=c_2$. The modal amplitudes g_n of the Green's function for this configuration are given by

(10) $$g_n(x,x_q,x_f,\omega_n)=2\frac{c_2}{\omega_n}\frac{\frac{\omega_n}{c_2}\rho_1 A\left(\omega_n,x_f\right)E(\omega,x_q)+\frac{\omega_n}{c_1}\rho_2 B\left(\omega_n,x_f\right)J(\omega_n,x_q)}{F'(\omega_n,x_f)}C\left(\omega_n,x\right)$$

with:

(11) $$F(\omega,x_f)=i\frac{\omega}{c_1}\rho_2 B\left(\omega,x_f\right)C\left(\omega,x_f\right)-i\frac{\omega}{c_2}\rho_1 A\left(\omega,x_f\right)D\left(\omega,x_f\right),$$

(12)
$$A(x,\omega)=R_0e^{i\frac{\omega}{c_1}x}+e^{-i\frac{\omega}{c_1}x} \qquad B(x,\omega)=R_0e^{i\frac{\omega}{c_1}x}-e^{-i\frac{\omega}{c_1}x}$$
$$C(x,\omega)=e^{i\frac{\omega}{c_2}x}+R_Le^{-i\frac{\omega}{c_2}(x-2L)} \qquad D(x,\omega)=e^{i\frac{\omega}{c_2}x}-R_Le^{-i\frac{\omega}{c_2}(x-2L)}$$
$$E(x,x_f,\omega)=e^{i\frac{\omega}{c_2}(x_f-x)}+e^{-i\frac{\omega}{c_2}(x_f-x)} \qquad J(x,x_f,\omega)=e^{i\frac{\omega}{c_2}(x_f-x)}-e^{-i\frac{\omega}{c_2}(x_f-x)}$$

where x_f is the position of the temperature jump which, in the following, will be set at the same position of the heat source, here x_q. For details about the procedure used for the derivation see references [2,4].

4. The integral governing equation

The acoustic velocity in the Rijke tube can be calculated from the Green's function and a heat release law, when the latter is of the form in Eq.(1). The following integral equation has been derived in [4]

(13) $$u(x_q,t)=\left.\frac{\partial\phi}{\partial x}\right|_{x=x_q}=-\frac{\gamma-1}{c^2}\int_{t'=0}^{t}\left.\frac{\partial G(x,x',t,t')}{\partial x}\right|_{x=x_q}q(t')dt'-\frac{\varphi_0}{c^2}\left.\frac{\partial G}{\partial x\partial t'}\right|_{\substack{x=x_q\\t'=0}}+\frac{\varphi_0'}{c^2}\left.\frac{\partial G}{\partial x}\right|_{\substack{x=x_q\\t'=0}}$$

where $\phi(x,t)$ is the velocity potential. The integral term represents the response of the acoustic field to the forcing by the unsteady local heat release rate $q(t)\delta(x-x_q)$. The last two terms are due to the initial conditions

(14) $$\left.\frac{\partial\phi(x,t)}{\partial x}\right|_{t=0}=\varphi_0'\delta(x-x_q) \qquad \text{and} \qquad \phi(x,t)|_{t=0}=\varphi_0\delta(x-x_q)$$

These represent the initial perturbation at the heat source, whose strength is given by the constants φ_0 and φ_0'.

4.1 Numerical solution: prediction of the time history

The integral equation can be iterated numerically to obtain the time evolution of the perturbation as follows. We define the integral

$$I_n(t) = \int_{t'=0}^{t-\Delta t} e^{i\omega_n t'} q(t')\,dt' + \int_{t'=t-\Delta t}^{t} e^{i\omega_n t'} q(t')\,dt' \tag{15}$$

so that, considering the modal form of G in Eq.(9), the integral equation (13) becomes

$$u_q(t) = -\frac{\gamma-1}{c^2}\Re\sum_{n=1}^{\infty} G_n e^{-i\omega_n t} I_n(t) - \frac{1}{c^2}\Re\sum_{n=1}^{\infty}(\varphi_0-\varphi_0')\frac{\varphi_0}{c^2} G_n e^{-i\omega_n t} \quad \text{with} \quad G_n = i\frac{\partial g_n}{\partial x}\bigg|_{\substack{x'=x_q \\ x=x_q}} \tag{16}$$

Taking a small time-step Δt, the integral I_n can be approximated as

$$I_n(t) = I_n(t-\Delta t) + q(t-\Delta t)\frac{1-e^{-i\omega_n \Delta t}}{i\omega_n} e^{-i\omega_n t} \tag{17}$$

Then we describe $q(t)$ using Eq.(1) and the correlation for the global heat release in Eq.(2), where the acoustic feedback is modelled by the dependency on the acoustic velocity perturbations. We obtain

$$q(t) = K\left[n_1 u_q(t-\tau) - n_0 u_q(t)\right] \text{ and } K = \frac{\bar{Q}}{\bar{U}S\bar{\rho}}\ , \tag{18}$$

where S is the tube cross section. Finally, setting an initial value for φ_0 and φ_0' to have $u_q(t=0)$, and observing that $I_n(t=0)=0$, we can iterate Eq.(17) for each subsequent time-step.

4.2 Modal analysis

In order to predict the response of the acoustic field to perturbations, we are going to investigate the stability of each acoustic mode. The acoustic velocity will be represented by a superposition of heat driven modes with amplitudes u_m and complex frequencies Ω_m

$$u(t) = \sum_{m=1}^{\infty} u_m e^{-i\Omega_m t} + u_m^* e^{i\Omega_m^* t} \tag{19}$$

Equating the modal acoustic velocity with equation (13), using the modal expression for the Green's function in equation (9) and the heat release law in (18), we obtain an expression for the heat driven frequencies and amplitudes. We will just report here the final result, more details on the derivation can be found in [2].

$$\sum_{n=1}^{\infty} \frac{G_n(n_1 e^{i\Omega_m \tau} - n_0)}{i(\omega_n - \Omega_m)} - \frac{G_n^*(n_1 e^{i\Omega_m \tau} - n_0)}{i(\omega_n^* + \Omega_m)} = \frac{2}{KB} \tag{20}$$

$$\sum_{m=1}^{\infty} \frac{u_m^*(n_1 e^{-i\Omega_m^* \tau} - n_0)}{i(\omega_n^* - \Omega_m^*)} + \frac{u_m(n_1 e^{i\Omega_m \tau} - n_0)}{i(\omega_n^* + \Omega_m)} = \frac{\varphi_0' + \varphi_o i\omega_n^*}{KBc^2} \tag{21}$$

Equations (20) and (21) show that the eigenmodes of the system depend on the parameters that describe the source, as the heater power K, and on the response of the source to acoustic perturbations, as the time lag τ and the gain. They are the *heat driven modes* of the system and are associated to complex frequencies, called *heat driven frequencies*. When acoustic feedback is present, the Ω_ms will differ from the ω_n with a non-negligible shift both in the real and imaginary part.

5. Stability maps

5.1 Predictions

The imaginary part of the Ω_ms carries the information on the stability of the system for a given

set of parameters, from which we can produce a stability map. To do so we proceed as follows. We initially calculate numerically the resonant frequencies of the system from the characteristic equation $F(\omega) = 0$ with F given in (11), using the Newton-Raphson method. Then we solve numerically equation (20), using equations (5) and (6) to find $n_0(A/\bar{U})$, $n_1(A/\bar{U})$ and $\tau(A/\bar{U})$ for different values of the flame position x_q and perturbation amplitude, and find the Ω_ms. The stability maps are then plotted for a single mode, Ω_1, in order to better analyse the dependence on system parameters.
In Figure 1 are shown the maps for the following situations: a) a sharp temperature jump at the heat source $\Delta T = 156°K$, with $T_1 = 304°K$, so that $c_1 = 350m/s$ and $c_2 = 430m/s$ with heater power constant $K = 3\times10^5\ Ws^{-1}kg^{-1}$, and the case in which the temperature can be approximated as uniform in the tube with b) $c = 350m/s$ and $K = 3\times10^5\ Ws^{-1}kg^{-1}$ c) $c = 390\ m/s$ and $K = 3\times10^5\ Ws^{-1}kg^{-1}$ d) $c = 350\ m/s$ and higher heater power, $K = 5\times10^5\ Ws^{-1}kg^{-1}$. We use the following values for the gain and time-lag parameters: $g_0 = 1.4$, $g_1 = 0.3$, $\tau_0 = 5\times10^{-3}s$ and $\tau_2 = 4.4\times10^{-3}s$. The length of the duct is $L = 2m$.

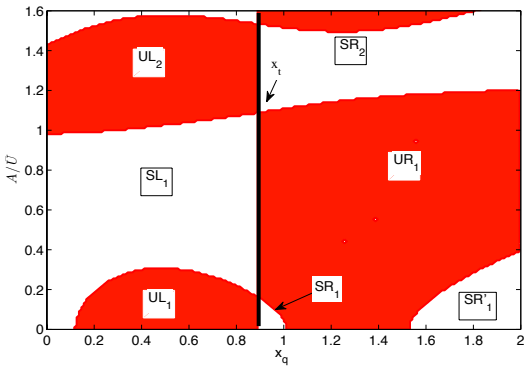

a) $c_1 = 350\frac{m}{s}$, $c_2 = 430\frac{m}{s}$, $K = 3\times10^5\ Ws^{-1}kg^{-1}$.

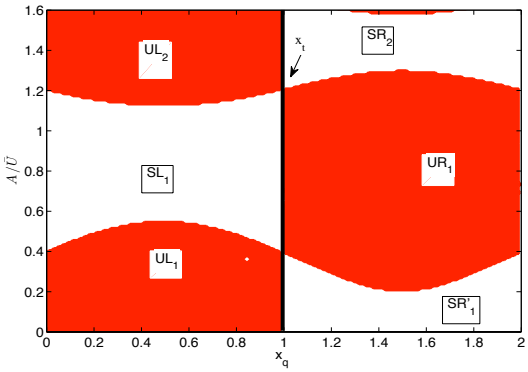

b) $c = 350\frac{m}{s}$, $K = 3\times10^5\ Ws^{-1}kg^{-1}$.

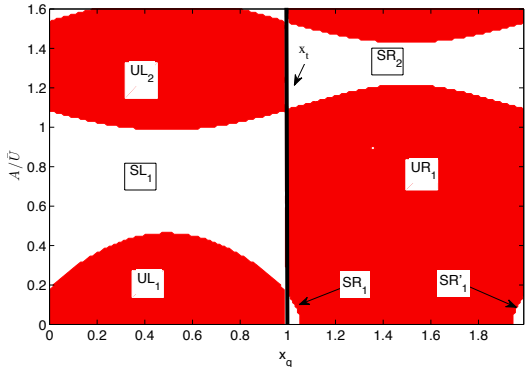

c) $c = 390\frac{m}{s}$ and $K = 3\times10^5\ Ws^{-1}Kg^{-1}$.

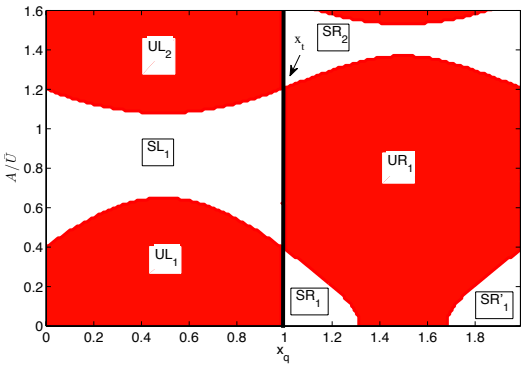

d) $c = 350\frac{m}{s}$ and $K = 5\times10^5\ Ws^{-1}Kg^{-1}$.

Figure 1. Stability maps for the heat source position x_q and perturbation amplitude $A/\ \bar{U}$ in a Rijke tube. $g_0 = 1.4$, $g_1 = 0.3$, $\tau_0 = 5\times10^{-3}s$ and $\tau_2 = 4.4\times10^{-3}s$. RED: unstable, WHITE: stable.

The *red* zones indicate, for each source position x_q, the range of amplitudes for which the system is unstable: when the system enters an unstable zone the amplitude of the perturbation grows in time until the border with a stable zone is found. When the system is in a stable zone (*white* colour) the amplitude drops to reach the border with a lower unstable zone. We observe that in Figure 1 a),c) and d) the stable zone SR_1 splits into two parts, separated by an unstable region. *The extension of this zone vary with heater power and temperature, becoming wider for increasing T and K.* Different types of interfaces between the stability zones can be identified in the maps. We can observe a *vertical transition line*, which determines the transition of the system from stable/unstable when the

source position value crosses x_t in each direction. The interface between a lower unstable zone and an upper stable zone (e.g. between UL_1 and SL_1) corresponds to *stable limit cycles*: any small variation of $A/\overline{U}$ from the interface value will bring the perturbation back to the initial amplitude. The interface between a lower stable zone and an upper unstable zone (e.g. between SL_1 and UL_2), instead, will correspond to *unstable limit cycles*: any small variation of $A/\overline{U}$ from the interface value will bring the system either in the lower stable zone, with a decrease of the perturbation amplitude, or in the unstable zone, where the perturbation will grow until the interface with the next stable zone.

5.2 Validation

In order to validate the stability maps, we have performed simulations of the time evolution of the acoustic perturbations for different values of x_q. The latter are based on the numerical solution of Eq.(13), iterating as described in section 4.1, and using the same parameters as for the stability maps. An example is shown in Figure 2a), where the time-history of the acoustic velocity is calculated at $x_q = 1.47\ m$. The simulations confirm at all points the stability behaviour in the maps: for each set of parameters, stable limit cycles are found whose amplitude corresponds, at each position x_q, to the stable limit cycle interface in the corresponding map.

The time evolution of the perturbation also shows that the frequency in the spectrum does not correspond to the modal frequency ω_1 (no-feedback) of the pipe for that specific source position and system parameters. This is shown in Figure 2b): the frequency associated to the first mode for the no-feedback case is $\omega_1 = 596\ rad\ s^{-1}$ while we find a peak in the spectrum at $565\ rad\ s^{-1}$. This is the previously mentioned frequency shift from ω_n to Ω_n, occurring as a result of the thermo-acoustic feedback. The latter does not only affect the imaginary part, but also the real part with variations up to 10% of the ω_n value.

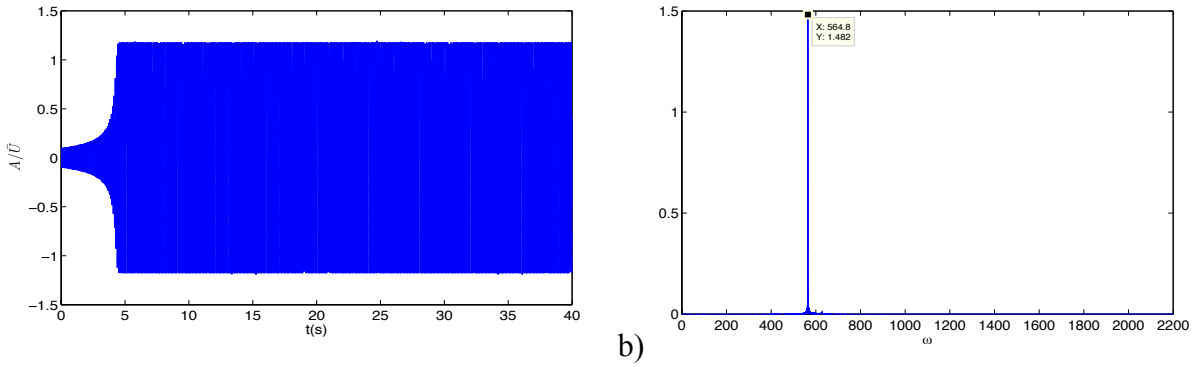

a) b)

Figure 2. Time evolution **a)** and spectrum **b)** for the heat source position x_q=147 cm and initial perturbation amplitude $u_0/A = 0.01$ in a Rijke tube with a temperature jump at $x_f = x_q$, with $c_1 = 350\ m/s$ and $c_2 = 430\ m/s$.

We emphasize that we never use the Ω_ms in the iteration procedure and time history calculations.

6. Hysteresis

6.1 Time-history calculations

Simulations of the time evolution can be also used to study the transition of the system from one stability zone to the next one, when the location of the heat source is varied.

To do so, we will proceed as follows: 1) A first simulation of the time evolution of the perturbation is performed for a heat source position close to the inlet $x_{q1} = 0.01m$ and initial perturbation amplitude $u_0/\overline{U} = 0.01$, for the time necessary for the perturbation to reach the saturation amplitude

(in general 10 s will be sufficient). We register the amplitude $A_1/\overline{U}$ of the perturbation at saturation. 2) We move the flame to the right by an interval Δx, to $x_{q2} = x_{q1} + \Delta x$ and we perform a new simulation with the new value of the flame position, using as the initial perturbation the value found in the previous simulation $u_0/\overline{U} = A_1/\overline{U}$. At the end of the simulation, we register again the perturbation amplitude $A_2/\overline{U}$. 3) We repeat step 2 until we reach the outlet of the pipe. At each position the saturation amplitude is recorded. 4) We repeat the whole procedure, steps 1-3, in the opposite direction, from the outlet to the inlet, so that $x_{qn} = x_{qn-1} - \Delta x$, and record $A_n/\overline{U}$ at each step. The results are plotted in Figure 3a) and b) for the case of a temperature jump at x_q and uniform temperature respectively. The solid line corresponds to the movement of the source position from left to right (L to R) and the dotted line from right to left (R to L) as indicated in the legend.

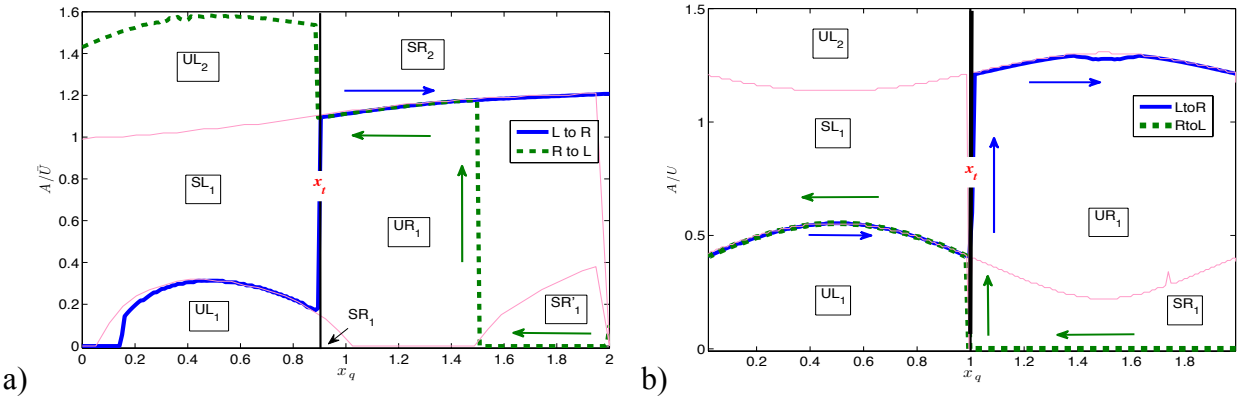

Figure 3. Perturbation amplitude $A/\overline{U}$ extrapolated from time-history simulation for different heat source positions x_q **a)** with a temperature jump at $x_f = x_q$, with $c_1 = 350\ m/s$ and $c_2 = 430\ m/s$ **b)** for uniform temperature $c = 350\ m/s$. Pink lines indicate the interface between stable/unstable zones.

6.2 Discussion

In Figure 3 a) and b) we observe two types of hysteresis which we will call *'type 1'* and *'type 2'*. Hysteresis of *'type 1'* is shown in Figure 3 b) by the blue arrows (forward direction) and green arrows (backward direction). If the heat source is initially placed at a point in the region SR_1, where the system is stable, any small perturbation will drop down to zero amplitude. Decreasing x_q of small steps (moving from right to left) the system will maintain its stability and move along the x_q axis until we reach the transition $x_q = x_t$. After crossing the transition line and entering zone UL_1, the amplitude grows since UL_1 is an unstable region. The growth stops when the system reaches the interface with the stable region SL_1, which corresponds to a stable limit cycle, and further decrease of x_q leads the system along this interface. If the heat source is moved in the reverse direction (left to right), starting from a point in the region UL_1, the system will move again along the interface between UL_1 and SL_1 until the transition line. At that point, there are two possibilities for the evolution of the perturbation: the system can enter the stable zone SR_1 or it can enter the unstable zone UR_1 above. Since the interface is curved and the variation of x_q is discrete, there is a preferred direction of the evolution, which is to enter UR_1. Then the amplitude grows until the interface with the stable region above UR_1. This is a stable limit cycle and further increase of x_q leads the system along this interface. This means that the system will not follow the same path as when the heat source position was moved from right to left. This type of hysteresis is also observed in Figure 3 a) (but not marked with arrows). It occurs at the transition line x_t and is entirely due to the convex/concave shape of the interface.

Hysteresis of *'type 2'* is shown in Figure 3 a) by the blue arrows (forward direction) and green arrows (backward direction). It covers a smaller portion of the pipe and is due to the fact that the low amplitude stability zone on the right of the transition line is divided into two parts, SR_1 and SR_1',

separated by an unstable region. Starting from a point in the region SR_1' and moving the heat source backwards from the outlet, the system is stable until $x_q = 1.49\,m$; after this point the system enters the unstable region UR_1. The amplitude then grows until it reaches the interface with zone SR_2. This is a stable limit cycle and further decrease of x_q leads the system along this interface. Assuming that we stop before x_t, and move forwards the heat source towards the outlet, the system will not re-enter the stable zone SR_1' but will continue to follow the stable limit cycle interface until the outlet. A similar result will be obtained moving from/towards SR_1. We notice that *the size of zones SR_1 and SR_1' determines the length of the pipe affected by hysteresis of second type*, therefore varying K or temperature parameters (see Section 4) it is possible to control this type of hysteresis.
We recall that we have made the assumption that, for each shift of Δx, the value of $A/\overline{U}$ before moving the flame is the same as the initial amplitude at the new position; different hysteresis path can be predicted assuming the perturbation is damped/increased as a consequence of the motion.

7. Conclusions

We have described thermo-acoustic oscillations and hysteresis in a Rijke tube, using a Green's function model. The stability analysis is performed with two methods: 1) Direct derivation of the eigenfrequencies in presence of thermo-acoustic feedback, considering separately the stability of each mode. This method allows the identification of the attractors of the systems (limit cycles) as a function of different parameters. 2) Iteration of the integral governing equation to obtain the time-history of the acoustic field. In this article we have considered just one mode in the integral equation to show that the solution is consistent with method 1), however higher modes can generally be included in the calculation to show the interaction between modes[2].

The Green's function approach has the advantage of providing a fast prediction of the stability behaviour of the system as a function of its parameters, while also giving a physical description of the process, which is fundamental for the control of thermo-acoustic feedback in combustors.

ACKNOWLEDGEMENTS

The presented work is part of the Marie Curie Initial Training Network Thermo-acoustic and aero-acoustic nonlinearities in green combustors with orifice structures (TANGO). We gratefully acknowledge the financial support from the European Commission under call FP7-PEOPLE-ITN-2012.

REFERENCES

1 Noiray, N. Linear and nonlinear analysis of combustion instabilities, application to mulitipoint injection systems and control strategies. PhD thesis, École Centrale Paris, Laboratory EM2C (2007).
2 Bigongiari, A. and Heckl, M. *Coupling of heat driven modes in the Rijke tube*, ICSV 21, Beijing, China, 13-17 July, (2014).
3 Heckl, M. Analytical model of nonlinear thermo-acoustic effects in a matrix burner, *n3l - Int'l Summer School and Workshop on Non-Normal and Nonlinear Effects in Aero- and Thermoacoustics*, Munich, Germany, 18 – 21 June, (2013).
4 Heckl, M. and Howe, M. S. *Journal of Sound and Vibration*, ***305***, *672-688, (2007)*.
5 Heckl, M. and Kosztin, B. *International journal of spray and combustion dynamics*, **5**(3), 243-272, (2013).
6 Kosztin, B., Heckl, M., and Jakob H. *International journal of spray and combustion dynamics*, **5**(1), 67-84, (2013).
7 Gopalakrishnan, E. A. and Sujith, R. I. Influence of system parameters and external noise on hysteresis characteristics of a horizontal Rijke tube, *n3l - Int'l Summer School and Workshop on Non-Normal and Nonlinear Effects in Aero- and Thermoacoustics*, Munich, Germany, 18 – 21 June, (2013).
8 Mariappan, S. and Sujith, R. I. Journal of Fluid Mechanics, **680**, 511-533, (2011).
9 Juniper, M. P. *International Journal of Spray and Combustion Dynamics* **4** (3), 217-238; (2012).